G-PFEM-aided derivation of undrained shear strength of organic clays from CPT data

Arthur Halleux[1], *Katia* Boschi[1#], *Luca* Flessati[2], and *Cristina* Jommi[1,2]

[1] *Department of Civil and Environmental Engineering, Politecnico di Milano*
piazza Leonardo da Vinci 32, 20113 Milan (Italy)
[2]*Department of Geoscience and Engineering, Delft University of Technology*
Stevinweg 1, 2628CN Delft (the Netherlands)
[#]*Corresponding author: katia.boschi@polimi.it*

ABSTRACT

Accurate evaluation of undrained shear strength of soils is crucial in geotechnical design and assessment. In the practice, undrained shear strength is obtained most frequently from CPT data, dividing the net cone tip resistance by a cone factor, N_{kt}. For organic soils, values between 8.6 and 15.3 are reported, depending on the stress history. The cone factor can be conditioned to the results of laboratory tests, although uncertainties remain on the variety of stress paths followed by the soil elements around the tip of the cone, compared to the ones tested in the laboratory. Non-uniqueness in the definition of the cone factor may lead to either unsafe or over-conservative choices, partly undermining both the reliability and the sustainability of the design. This contribution analyses numerically the inversion technique used to determine the undrained shear strength of organic clays, exploiting data from an extensive in situ and laboratory investigation. The adopted constitutive model was calibrated on the results of laboratory tests. Cone penetration tests were simulated performing coupled hydro-mechanical numerical analyses via G-PFEM, developed in the last decade at CIMNE-UPC. The role played by initial stress state and previous stress history upon stress distribution at failure, cone factor and sleeve friction is discussed. The numerical results suggest how the sleeve friction could be used to condition the cone factor depending on the over-consolidation ratio and demonstrate how combining the different available CPT readings with the aid of numerical results may reduce the uncertainty in the estimation of undrained shear strength.

Keywords: CPT; numerical modelling; organic clay; undrained shear strength; cone factor.

1. Introduction

Cone penetration tests (CPTs) are often the basis for geotechnical soil characterisation. These tests provide cost-effective, repeatable, nearly continuous profiles, widely employed to determine the soil stratigraphy, estimate hydro-mechanical properties of soils (Mayne, 2007a) and assist the geotechnical design (e.g., Lehane et al., 2022).

In case of clayey soils, CPTs are often used to estimate soil undrained shear strength. However, the process, which allows calculating the undrained shear strength from net tip resistance q_{net} passes through the use of a transformation cone factor N_{kt} (Lunne et al., 1997; Mayne et al., 2018). According to the literature (Low et al., 2010), the latter ranges between 8.6 and 15.3 for organic clays. In the absence of further information, the rather wide range of possible values implies that the chosen undrained strength can be severely either over- or under-estimated. Depending on the case, the uncertainty leads to either unsafe or over-conservative design, which makes questionable the reliability of a CPT-based design.

Literature studies on CPT are mainly focused on discussing the role of material properties, both strength and stiffness, on cone factor (Yu & Mitchell, 1998). These contributions do not address explicitly the role of both the previous stress history and the initial stress state on the CPT results. Moreover, in general, the estimation of soil strength properties from CPT data is based only on cone tip resistance readings (Teh & Houlsby, 1991). Sleeve friction is usually employed, instead, to the purpose of soil classification (Robertson, 2009).

Mayne (2007b) attempted to enhance the interpretation of CPT readings by developing an analytical solution based on modified Cam-Clay. This solution, however, is based on the simplifying assumption of considering an expansion of a spherical cavity, which may not be representing accurately the true failure mechanism

In this work, with the results of numerical analyses, an attempt to improve the interpretation of CPT test readings for organic clays is proposed, by combining cone tip resistance, q_t, and sleeve friction, f_s, measurements. The study aims to investigate whether numerical results can be used to condition the transformation factor, N_{kt}, to the stress state and stress history of the soil, to improve the reliability of the undrained shear strength, s_u, obtained from CPTs.

The results of an extensive experimental investigation including both in situ and laboratory tests on an organic clay underpin the study. A series of large displacements coupled hydro-mechanical axisymmetric numerical analyses reproducing CPTs were performed (§2). The soil mechanical behaviour was reproduced by using a strain hardening constitutive relationship calibrated on

the laboratory test results. Different stress history and initial stress state were considered, and the numerical results were used to identify the relationships between over-consolidation ratio, sleeve friction and cone tip resistance. These relationships were used to estimate undrained shear strength under triaxial conditions (§3) and validated with the field data (§4).

2. Numerical modelling

Cone penetration testing is an insertion problem into a soil domain, involving large displacements and strains, hydro-mechanical coupling and interaction between the cone and the surrounding soil. The simulation of such a test requires an advanced numerical approach capable of addressing these issues. In this work, the CPTs are reproduced by using the G-PFEM (Geotechnical code based on Particle Finite Element Method), developed in the last decade at CIMNE-UPC (Monforte et al., 2017a; 2018; 2022) and implemented in Kratos Multiphysics (Dadvand et al., 2010). The suitability of this numerical approach in reproducing CPTs was already demonstrated in many numerical works (Monforte et al., 2021; Hauser & Schweiger, 2021; Oliynyk et al., 2021; Boschi et al., 2024).

A continuous regeneration of the finite element mesh covering the domain is one of the key aspects of G-PFEM. H-adaptive techniques are used to refine the discretisation in areas where localisation is likely to take place as well as mesh smoothing procedures to enhance mesh quality. A fully coupled hydromechanical formulation is adopted. The domain is discretised with mixed stabilised linear triangles having displacements, Jacobian and water pressure as degrees of freedom (Monforte et al., 2017b). To alleviate mesh-dependency of the solution due to strain-softening, a non-local regularization technique is also employed (Monforte et al., 2019). The cone–soil interface contact conditions are mathematically expressed as a set of restrictions on the solution and the interaction forces are derived from those constraints (Monforte et al., 2017b). Along the direction normal to the contact surface, (i) only compressive normal force is allowed, (ii) penetration of the two bodies is not allowed and (iii) null normal force is enforced when the bodies are not in contact. Along the tangential direction, the contact condition is elastic-plastic and the contact slip is controlled by an interface friction angle, δ.

2.1. Model description

The geometry of the problem (Fig. 1) is assumed to be axisymmetric. The frictional cone is modelled according to ISO standard 22476-1:2012: with a radius R = 17.84 mm, an apex angle α = 60°, a cylindrical friction sleeve with the same radius as the cone basis and a height H = 134 mm. The soil-cone interface friction angle is δ = 15°, corresponding to δ/ϕ' = 0.43, where ϕ' is the soil friction angle. The cone is initially positioned at a depth of $11R$ and pushed at a standard velocity v of 2 cm/s. Boundary conditions include nil vertical displacements at the bottom and nil radial displacements along the vertical boundaries. A uniform initial effective state of stress is imposed: the initial vertical effective stress σ'_{v0} is imposed through the application of a surcharge q at the top of the domain, whereas the initial horizontal effective stress σ'_{h0} is directly imposed through at rest lateral earth pressure coefficient $k_0 = (1 - sin\,\phi') \cdot OCR^{0.5}$. The initial pore water pressure u_0 is assumed to be zero. Drainage is allowed through the bottom and top boundaries, whereas the vertical boundaries are impervious to water.

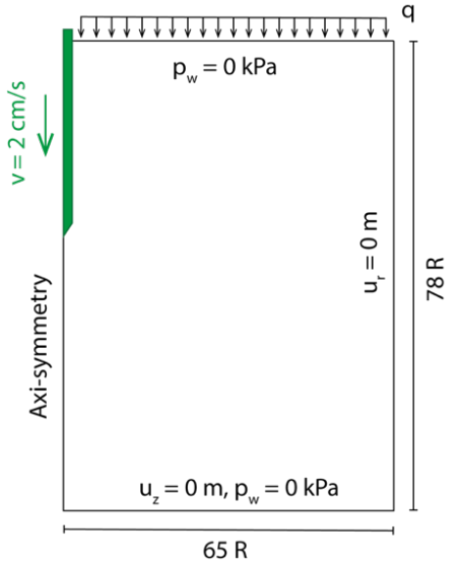

Figure 1. Simulation of CPT tests: numerical model scheme.

A preliminary study on the influence of the boundary conditions was carried out. For radial and vertical length of the cylindrical domain equal to $65R$ and $78R$, respectively, the perturbation induced by the cone insertion is negligible at the boundaries. The initial element number is 6057, but, since the numerical method is based on a continuous re-meshing, the number of elements progressively changes during the numerical simulation.

2.2. Constitutive law

Within the framework of large-strain elasto-plasticity, the constitutive model employed is a version (Mánica et al., 2022) of the isotropic, critical state-based model CASM (Yu, 1998), already implemented in G-PFEM code (details are given in Boschi et al., 2024).

The elastic part is described by a hyper-elastic law (Borja & Tamagnini, 1998), in which the bulk modulus depends linearly on the mean effective stress, and the shear modulus is constant. The value of the latter is fixed on the initial value of the mean effective stress assuming an initial Poisson's ratio equal to 0.35.

The values of the model parameters, which describe the shape of the yield surface, have been chosen to approximate the modified Cam Clay (MCC) soil model (n = 2 and r = 2). The hardening law is the classical isotropic volumetric strain rule of critical state soil models and the stress-dilatancy relation by Mánica et al. (2022) is used, to fit the plastic flow rule of MCC. The slope of Critical Stale Line (CSL) depends on the Lode's angle. The shape of the yield function in the deviatoric plane is given by Abbo et al. (2011), following a smoothed Mohr-Coulomb-like shape.

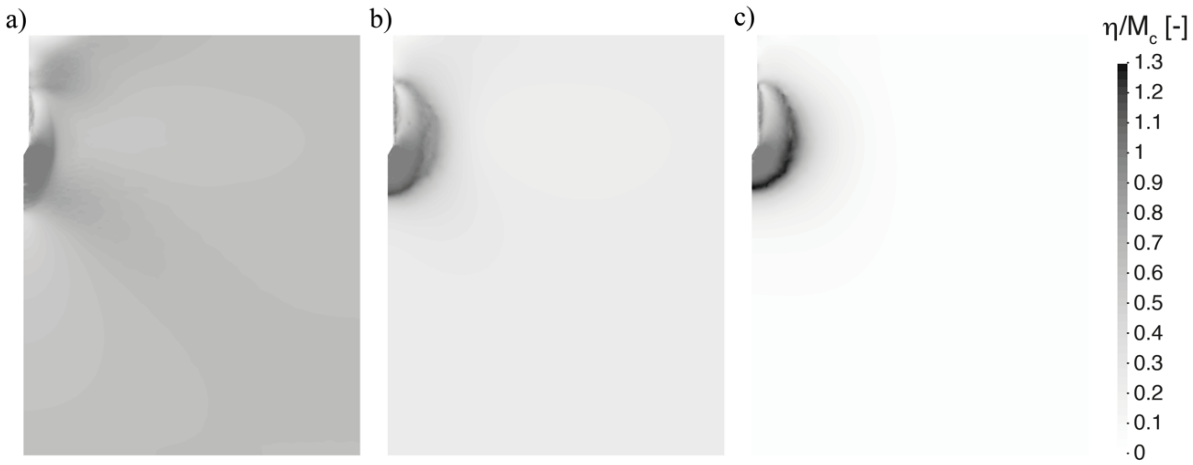

Figure 2. Contours of normalised obliquity (η/M_C) at penetration $z = 10R$: a) $OCR = 1$; b) $OCR = 2.5$; c) $OCR = 4$.

The ratio R_{M_θ} between the CSL slope under triaxial extension and compression (M_E and M_C, respectively) can be assigned.

The isotropic consolidation line (ICL) and the critical state line (CSL) are defined by straight lines in the bi-logarithmic compression plane ($\ln(1+e) - \ln(\pi')$, where e is the void ratio and π' is the Kirchoff mean effective stress) characterised by a slope λ^* (Hashiguchi & Ueno, 1977; Butterfield, 1979). In the same plane, the slope of the reloading line is κ^*. It is worth noting that, in the stress range relevant for this work, this formulation is practically coincident with the small-strain semilogarithmic formulation usually employed to interpret the experimental results (Reid et al., 2021). The two models almost coincide as long as: (i) the slope of the CSL in the $e - \ln(p')$ space is $\lambda = \lambda^*(1+N)$, where p' is the Cauchy mean effective stress and N the void ratio belonging to the ICL at a reference mean effective stress p'_r; (ii) the slope of the reloading curve in the e - $\ln(p')$ space is $\kappa = \kappa^*(1+N)$; (iii) the void ratio at p'_r belonging to CSL is $\Gamma_r = N - (\lambda - \kappa)\ln r$.

The initial value of the hardening variable p_0^* is imposed by considering a maximum vertical effective stress $\sigma'_{v,max} = OCR \cdot \sigma'_{v0}$ and $\sigma'_{h,max} = (1 - sin\,\phi') \cdot \sigma'_{v,max}$.

The constitutive model parameters adopted in the numerical simulations were calibrated on the results of laboratory tests performed on organic clay samples retrieved at Leendert de Boerspolder (Ponzoni, 2017; Muraro, 2019). The input data are summarised in Table 1.

Table 1. Void ratio N belonging to ICL at p'_r = 1 kPa, slope λ of the CSL in the $e - \ln(p')$ space, slope κ of the reloading curve in the same plane, slope of the CSL in triaxial compression M_C and ratio R_{M_θ}.

N [-]	λ [-]	κ [-]	M_C [-]	R_{M_θ} [-]
4.2	0.214	0.023	1.42	0.74

The soil hydraulic behaviour is assumed to follow Darcy's law and the hydraulic conductivity k is assumed to be isotropic and independent from the void ratio, with a constant value of $5 \cdot 10^{-8}$ m/s. A series of preliminary numerical tests, performed varying the hydraulic conductivity, demonstrated that for $k = 5 \cdot 10^{-8}$ m/s the system response is "practically undrained" (according to Boschi et al. 2023). For the case analysed, then, the excess pore water pressure dissipation is negligible with respect to the excess pore pressure generated by the cone advancement.

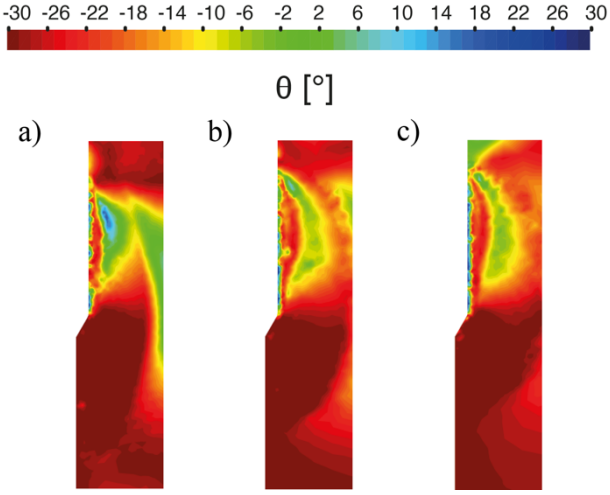

Figure 3. Contours of Lode's angle at the cone tip proximity, corresponding to a penetration $z = 10R$: a) $OCR = 1$; b) $OCR = 2.5$; c) $OCR = 4$.

3. Numerical results

The simulations return profiles of q_t and f_s. The former is determined as the force on the cone tip divided by the projected cone tip area, the latter is computed from tangential forces along a length of $7.5R$ right behind the cone tip. After $10R$ of penetration, q_t and f_s are no longer affected by the upper boundary conditions. These constant values were used in the discussion of the results.

In the following, the attention is focussed on the influence of the initial stress state and the previous stress history, as a function of OCR, on the CPT readings.

In Fig. 2, the contours of stress obliquity η normalised to M_C are plotted as a function of OCR. It is worth noting that, in the analyses, the different values of OCR were obtained by assigning the same maximum effective stress $\sigma'_{v,max}$ = 32 kPa, and unloading at decreasing values of σ'_{v0}. The portions of the domain for which $\eta/M_C \geq 1$ are either at peak failure or at critical state and significantly differ for the 3 cases. For $OCR = 4$, the sub-domain at failure has an almost spherical shape and involves both the soil under the cone and the one in the proximity of the shaft. The radius of this sphere is approximately equal to $6.5R$. For $OCR = 1$, the portion at failure is smaller and mainly positioned under the cone tip. For $OCR = 2.5$, the domain at failure is intermediate between the two other cases and assumes a nearly elliptical shape.

The difference in the failure mechanisms is due to both a different material response in the proximity of the cone tip (strain hardening for $OCR = 1$ and strain softening for $OCR = 4$) and a different initial value of η. For $OCR = 4$, the initial η value is almost 0 (the initial state of stress is practically isotropic) promoting the development of an almost spherical failure domain, similar to the one considered by Mayne (2007b) in his analytical derivation. However, it may be observed that this is not the case anymore at lower values of OCR, as already observed.

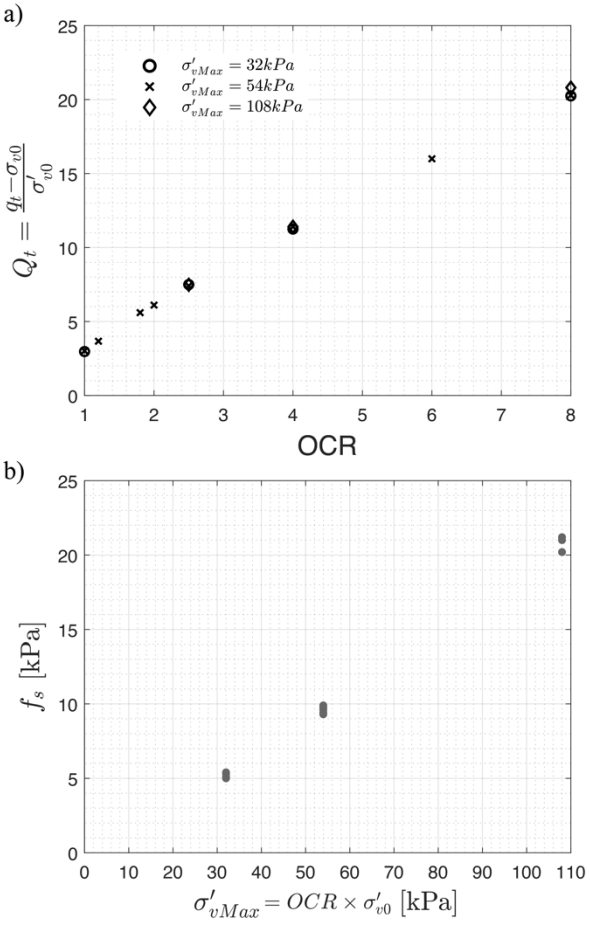

Figure 4. Evolution of a) normalised q_{net} with OCR and b) sleeve friction with $\sigma'_{v,max}$.

In Fig. 3, the same results are compared in terms of contours of Lode's angle θ (θ = -30° and 30° represent triaxial compression and extension, respectively). For the sake of clarity, only the part of the domain close to the cone tip is reported. Independently from OCR, the soil beneath the cone is under triaxial compression (as also found by Monforte et al., 2023). On the contrary, in the proximity of the shaft, θ assumes values similar to those of simple shear conditions, with θ approaching 0. The overall shapes of θ distributions are similar to the ones observed in terms of η: for $OCR = 1$, the shape of this subdomain is more elongated towards the vertical direction compared to the more spherical one shown in the $OCR = 4$ case.

In Fig. 4a, the results of 15 numerical simulations considering different values of OCR and $\sigma'_{v,max}$ are reported in terms of normalised net cone tip resistance q_{net}/σ'_{v0}, where $q_{net} = q_t - \sigma_{v0}$, and σ_{v0} is the initial total vertical stress, as a function of OCR. In Fig. 4b, the corresponding results are reported in terms of variation of sleeve friction f_s with $\sigma'_{v,max} = OCR \cdot \sigma'_{v0}$. The numerical results clearly show that the previous history influences both normalised q_{net} and f_s.

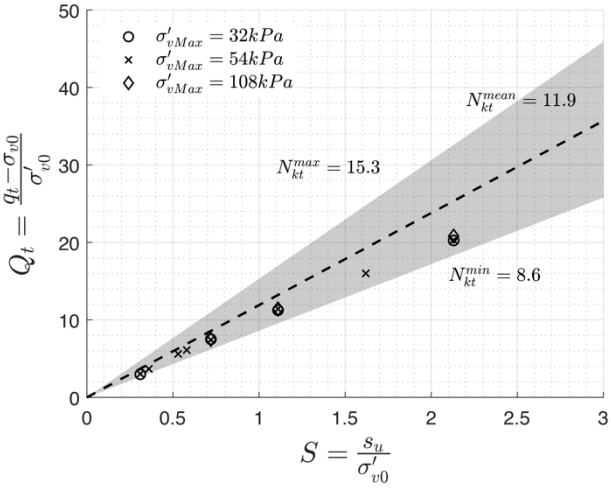

Figure 5. Evolution of normalised q_{net} with normalised s_u.

As previously mentioned, in the current practice, q_{net} values are used to derive the undrained strength of clayey soil by adopting a transformation factor $N_{kt} = q_{net}/s_u$. In Fig. 5, the variation of q_{net}/σ'_{v0} with s_u/σ'_{v0}, obtained from the numerical analyses, is plotted. Straight lines representing N_{kt} = 8.6, 11.9 and 15.3 are also plotted. These represent a lower, a mean and an upper value identified for organic clays in the literature (Low et al., 2010).

The undrained shear strength obtained from the numerical analyses depends on the adopted soil constitutive model with the calibrated parameters (reported in Table 1 for the case under exam), the stress path, the initial stress state and the previous history (through both k_0 and p_0^*).

For a triaxial compression stress path, (θ = -30°; Fig. 3), s_u can be calculated by means of the following analytical expression, obtained by integrating the constitutive law over the path assuming undrained response:

$$s_u/\sigma'_{v0} = \frac{M_c}{2} \cdot \frac{1+2k_0}{3} \cdot \left[r \cdot \frac{(1+2k_0)\,\sigma'_{v0}}{3 \cdot p_0^*} \right]^{-\frac{\lambda-\kappa}{\lambda}} \quad (1)$$

It is possible to demonstrate that p_0^* linearly depends on σ'_{v0}, implying that s_u/σ'_{v0} is constant for the same previous history (OCR).

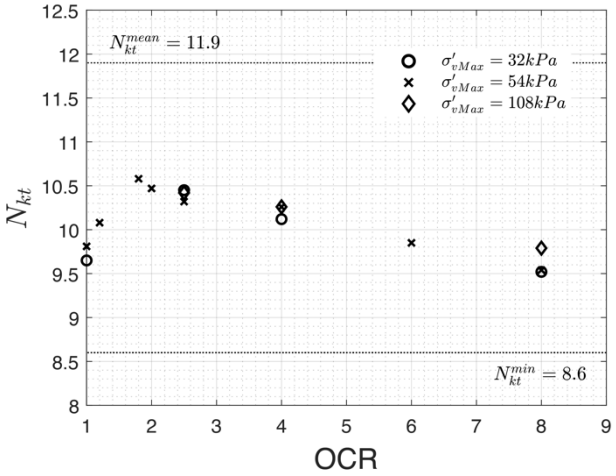

Figure 6. Evolution of N_{kt} with OCR.

The numerical results put in evidence that, for the same OCR value, also q_{net}/σ'_{v0} is almost constant (Fig.4a), implying that N_{kt} is not a function of σ'_{v0}. On the contrary, a non-linear dependence of q_{net} on s_u (Fig. 5) is observed by changing OCR, which implies that N_{kt} depends on the previous stress history, as illustrated in Fig. 6. This dependency is due to both the shape of the failure mechanism and the soil behaviour in the proximity of the cone tip. For $OCR < 1.7$, initial state parameter $\psi > 0$ (Been and Jefferies, 1985), the soil tends to exhibit a contractive behaviour and N_{kt} increases with OCR. Conversely, for $OCR > 1.7$, $\psi < 0$, the soil tends to exhibit a dilative behaviour and N_{kt} decreases with OCR. The maximum of the curve is obtained for $OCR = 1.7$, the value for which triaxial compression undrained stress paths reach critical state at first yielding.

It is worth noting that the specific function relating N_{kt} to OCR is expected to depend on soil properties. However, the discussion of this dependency is not included in this contribution, which is underpinned by a specific data set (Table 1). The values of N_{kt} found for the organic clay under investigation are close to the lower bound proposed by Low et al. (2010). If the safe-side upper bound N_{kt} = 15.3 (Low et al., 2010) were used for this clay, the undrained shear strength would be underestimated by approximately 30%, leading to over-conservative design choices and partly undermining sustainability.

4. Practical implementation

As previously discussed, N_{kt} is a function of OCR. As a consequence, it is not possible to provide an accurate estimation of s_u with q_t readings only, or with an average transformation factor based on previous experience. However, as shown in Fig. 4b, the OCR influences both Q_t and f_s. Exploiting these results, it may be suggested that the combined use of Q_t and f_s readings would allow for a more reliable choice of N_{kt} depending on the OCR.

Once the OCR is estimated from the sleeve friction reading, N_{kt} can be conditioned to the graph describing its dependence from OCR for the specific material. Eventually, s_u can be obtained by using the calibrated value of N_{kt}.

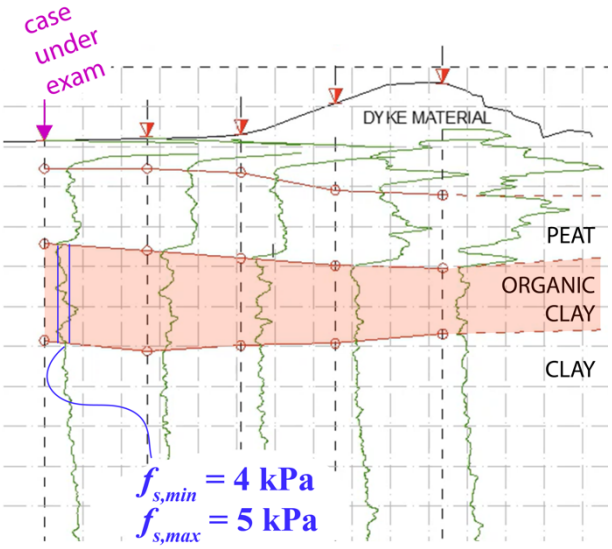

Figure 7. Schematisation of the Leendert de Boerspolder site.

The procedure is illustrated by applying it to the set of data coming from the Leendert de Boerspolder site, which includes both CPTs (Fig. 7; de Gast, 2020) and laboratory tests results (Ponzoni, 2017; Muraro, 2019). The case study and some of the tests performed on this site are presented and discussed in Jommi et al. (2021) and de Gast et al. (2021). In particular, the organic clay layer in the polder (Fig. 7) is considered.

The experimental f_s measurements, corresponding to σ'_{v0} approximately equal to 8 kPa, ranges between 4 and 5 kPa (Fig. 7). For f_s = 5 kPa, the corresponding value of $\sigma'_{v,max}$ in accordance with the numerical results is 32 kPa (Fig. 8a), resulting in $OCR = 4$. The result is in very close agreement with that experimentally derived by interpreting laboratory data ($OCR \simeq 3.8$) by Ponzoni (2017) and Muraro (2019).

The numerical value of N_{kt} corresponding to the predicted OCR value is equal to 10.1 (Fig. 8b). By calculating s_u using the derived value of N_{kt} and the experimental values of q_{net} ranging between 80 and 90 kPa (de Gast, 2020), an undrained shear strength s_u ranging between 7.9 and 8.9 kPa is obtained. Once more, these values match the ones obtained from undrained triaxial tests in the laboratory, ranging between 7.4 and 9 kPa (Ponzoni, 2017).

5. Conclusions

Results of G-PFEM simulations were analysed to evaluate the influence of the initial stress and the previous stress history on the results of CPTs performed in organic clay. The results show that both the cone factor and the sleeve friction can be directly related to the initial stress and to the OCR. Based on the numerical results, the in-

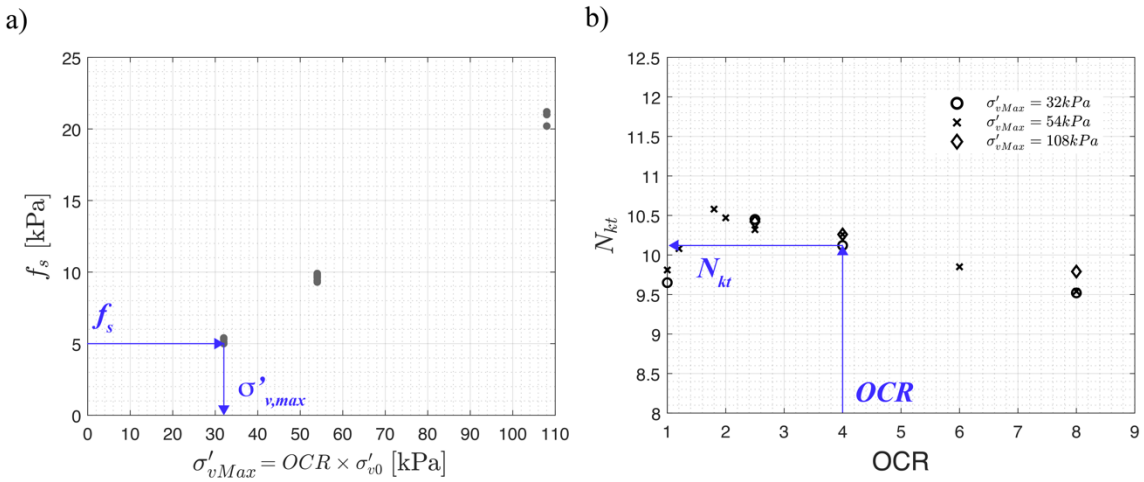

Figure 8. Practical application: a) $\sigma'_{v,max}$ prediction from f_s value; b) N_{kt} prediction from OCR value.

situ readings of f_s can be used to estimate the OCR, on which N_{kt} depends. The derived N_{kt} is adopted to transform the cone tip resistance reading into a reliable value of undrained strength. The novel proposal has been validated with reference to a site, where a complete set of data covering both in situ and laboratory tests is available. The dependency of sleeve friction and cone factor on OCR was obtained numerically, by calibrating the adopted constitutive model on the available set of laboratory data and numerically simulating CPT tests for various initial stress and previous stress histories.

Acknowledgements

The financial support of the Dutch Organisation for Scientific Research (NWO) to the projects "Sustainable Dykes" (TWM.BL.019.010) and "Reliable Dykes" (number 13864) is gratefully acknowledged.

References

Abbo, A. J., Lyamin, A. V., Sloan, S. W., & Hambleton, J. P. 2011. "A C2 continuous approximation to the Mohr–Coulomb yield surface". International Journal of solids and Structures, 48(21), 3001-3010.

Been, K. and Jefferies, M.G., 1985. A state parameter for sands. *Géotechnique*, *35*(2), pp.99-112.

Borja, R. I. and C. Tamagnini 1998. "Cam–clay plasticity, part III: Extension of the infinitesimal model to include finite strains". Comp. Meth. Appl. Mech. Engng. 155, 73–95.

Boschi, K., Monforte, L., Arroyo, M., Carbonell, J. M. & Gens, A. 2023. "Effects of drainage conditions on state parameter inversion from CPTu". NUMGE 2023. https://doi.org/10.53243/NUMGE2023-394

Boschi, K., Arroyo, M., Monforte, L., Carbonell, J. M., & Gens, A. 2024. "Coupled hydromechanical modelling of cone penetration in layered liquefiable soils". Géotechnique, 1-38. https://doi.org/10.1680/jgeot.23.00164

Butterfield, R. A. (1979). A natural compression law for soils (an advance on e–log p′). Géotechnique 29, No. 4, 469–480, https://doi.org/10.1680/geot.1979.29.4.469

Dadvand, P., Rossi, R., Oñate, E., 2010. "An object-oriented environment for developing finite element codes for multidisciplinary applications". Arch. Comput. Methods Eng. 17 (3), 253–297.

de Gast, T. 2020. "Dykes and Embankments: a Geostatistical Analysis of Soft Terrain". PhD dissertation, Delft University of Technology, http://repository.tudelft.nl/

de Gast, T., Hicks, M.A., Van den Eijnden, A.P. and Vardon, P.J., 2021. "On the reliability assessment of a controlled dyke failure". Géotechnique, 71(11), pp.1028-1043.

Hashiguchi, K. & Ueno, M. 1977. "Elasto-plastic constitutive laws of granular materials". In Constitutive equations of soils, proceedings of special session 9 of the 9th ICSMFE (eds S. Murayama and A. N. Schofield), pp. 72–83.

Hauser, L., & Schweiger, H. F., 2021. "Numerical study on undrained cone penetration in structured soil using G-PFEM." Computers and Geotechnics 133, 104061.

Jommi, C., Chao, C.Y., Muraro, S. and Zhao, H.F., 2021. "Developing a constitutive approach for peats from laboratory data". Geomechanics for Energy and the Environment, 27, p.100220.

Lehane, B. M., Bittar, E., Lacasse, S., Liu, Z. & Nadim, F. 2022. "New CPT methods for evaluation of the axial capacity of driven piles". Cone penetration testing 2022 (eds G. Gottardi and L. Tonni), 3–15. Boca Raton, FL, USA: CRC Press.

Low, H. E., Lunne, T., Andersen, K. H., Sjursen, M. A., Li, X., & Randolph, M. F. 2010. "Estimation of intact and remoulded undrained shear strengths from penetration tests in soft clays". Géotechnique, 60(11), 843-859.

Lunne, T., Robertson, P.K., & Powell, J.M. 1997. "Cone penetration testing in geotechnical practice". Blackie Academic & Professional, London, UK

Mánica, M.A., Arroyo, M., Gens, A., and Monforte, L. 2022. "Application of a critical state model to the Merriespruit tailings dam failure". Proceedings of the Institution of Civil Engineers - Geotechnical Engineering. https://doi.org/10.1680/jgeen.21.00001

Mayne, P.W. 2007a. "Cone penetration testing". Washington, DC, USA: Transportation Research Board, 368.

Mayne, P.W. 2007b. "In-situ test calibrations for evaluating soil parameters". Characterization & engineering properties of natural soils, 3, pp.1601-1652.

Mayne, P. W., & Peuchen, J. 2018. "Evaluation of CPTU N_{kt} cone factor for undrained strength of clays". Cone Penetration Testing, 423-429

Monforte, L., Arroyo, M., Carbonell, J.M., Gens, A. 2017a. "Numerical simulation of undrained insertion problems in geotechnical engineering with the particle finite element method (PFEM)". Comput. Geotech. 82, 44–156.

Monforte, L., Carbonell, J. M., Arroyo, M., & Gens, A. 2017b. "Performance of mixed formulations for the particle

finite element method in soil mechanics problems". Computational Particle Mechanics, 4(3), 269-284.

Monforte, L., Arroyo, M., Carbonell, J. M., & Gens, A. 2018. "Coupled effective stress analysis of insertion problems in geotechnics with the particle finite element method". Computers and Geotechnics, 101, 114-129.

Monforte, L., Ciantia, M. O., Carbonell, J. M., Arroyo, M. & Gens, A. 2019. "A stable mesh-independent approach for numerical modelling of structured soils at large strains". Comput. Geotech. 116, 103215.

Monforte, L., Gens, A., Arroyo, M., Mánica, M. and Carbonell, J.M., 2021. "Analysis of cone penetration in brittle liquefiable soils". Computers and Geotechnics, 134, p.104123.

Monforte, L., Arroyo, M., Carbonell, J. M., & Gens, A. 2022. "Large-strain analysis of undrained smooth tube sampling". Géotechnique, 72(1), 61-77.

Muraro, S. 2019. "The deviatoric behaviour of peat: a route between past empiricism and future perspectives". Ph.D. thesis, Delft University of Technology, http://repository.tudelft.nl/.

Oliynyk, K., Ciantia, M. O., & Tamagnini, C. 2021. "A finite deformation multiplicative plasticity model with non–local hardening for bonded geomaterials". Computers and Geotechnics 137, 104209.

Ponzoni, E. 2017. "Historical constructions on natural silty soils accounting for the interaction with the atmosphere". Ph.D. thesis, Università degli Studi di Brescia.

Reid, D., Fourie, A., Ayala, J. L., Dickinson, S., Ochoa-Cornejo, F., Fanni, R. & Suazo, G. (2021). Results of a critical state line testing round robin programme. Géotechnique 71, No. 7, 616–630, https://doi.org/10.1680/jgeot.19.P.373

Robertson, P. K. 2009. "Interpretation of cone penetration tests—a unified approach". Canadian geotechnical journal, 46(11), 1337-1355.

Teh, C. I., and Houlsby, G. T. 1991. "An analytical study of the cone penetration test in clay." Geotechnique, 41(1), 17–34.

Yu, H.S., 1998. "CASM: A unified state parameter model for clay and sand. International". Journal for Numerical and Analytical Methods in Geomechanics 22, 621–653.

Yu, H. S., and Mitchell, J. K. (1998). "Analysis of cone resistance: A review of methods." J. Geotech. Geoenviron. Eng., 124(2), 140–149.